# Voltage Linearity Improvement of HfO₂-Based Metal–Insulator–Metal Capacitors with H₂O Prepulse Treatment

**Cheng-Ming Lin,**[a,b] **Yen-Ting Chen,**[a,b] **Cheng-Hang Lee,**[a,b] **Hung-Chih Chang,**[a,b] **Wei-Chiang Chang,**[a,c] **Huan-Lin Chang,**[a,b] **and C. W. Liu**[a,b,c,*,z]

*[a]Department of Electrical Engineering, [b]Graduate Institute of Electronics Engineering, and [c]Graduate Institute of Photonics and Optoelectronics, National Taiwan University, Taipei 10617, Taiwan*

The effects of in situ H₂O prepulse treatment on the bottom Pt electrode of a metal–insulator–metal (MIM) capacitor prior to HfO₂ atomic layer deposition process were investigated for the first time. The cross-sectional transmission electron microscopy (TEM) shows a thicker HfO₂ layer on the 5-cycle prepulsed Pt surface than that on the no-prepulsed Pt surface. According to TEM results and grazing incidence X-ray diffraction, it shows that the polycrystallization of the HfO₂ film with the predominant monoclinic phase can be suppressed when the bottom Pt electrode was pretreated by H₂O pulses. X-ray photoelectron spectroscopy indicated that the surface of the bottom Pt electrode was hydroxylated, which was considered to be able to facilitate metallorganic precursor bonding with –OH groups on the Pt surface. Atomic force microscopy reveals that the roughness on the HfO₂ film surface decreases with increasing H₂O prepulse cycles. Symmetrical leakage current density versus applied voltage ($J_g$–$V$) curves were observed. Lower capacitance densities and reduced $J_g$ of the H₂O-prepulsed samples can be attributed to a thicker dielectric layer. A HfO₂ MIM capacitor has a capacitance density of 8.7 fF/μm², the quadratic voltage coefficient of capacitance ($\alpha$) of 499 ppm/V², and $J_g$ of $4.8 \times 10^{-8}$ A/cm² at 1 V and at room temperature.
© 2010 The Electrochemical Society. [DOI: 10.1149/1.3517173] All rights reserved.

Metal–insulator–metal (MIM) capacitor is essential to integrate radio frequency (rf) and analog functions into integrated circuits (ICs). It is also attracting great attention recently for the applications on dynamic random access memory (DRAM). In order to meet the requirements of the International Technology Roadmap for Semiconductors,[1] new materials with a high dielectric constant (high-κ) should be utilized to replace the conventional dielectrics, such as SiO₂ (κ ∼ 3.9) and Si₃N₄ (κ ∼ 7),[2-4] to obtain a high capacitance density and a low leakage current density. Among several high-κ material candidates, the HfO₂-based gate stack of a metal-oxide-semiconductor field-effect transistor was implemented into commercial IC chips due to the excellent electrical properties and high thermal stability.[5] Pulsed laser deposition, atomic layer deposition (ALD), and magnetron sputter deposition were reported to grow thin HfO₂ film for the MIM devices.[6-10] With the advantages of accurate film thickness control, excellent conformity, and reproducibility, the ALD technique seems to be the most useful technology for the MIM applications.

Titanium nitride (TiN) and tantalum nitride (TaN) are commonly used in metallization technologies in the back end process.[9] However, the formation of a native surface oxide at room temperature and/or additional interfacial layer during postannealing treatment may degrade the electrical performance.[11] In spite of some drawbacks, such as high cost and etching difficulty, Pt, with a large work function, low resistance, and high oxidation resistance, is attractive for the MIM electrode.[12] Chang et al.[13] reported that the lack of lone-pair electrons on the Pt surface could lead to a weak chemisorption between the metallorganic (MO) precursor and the Pt surface. A hydroxylated treatment on the Pt electrode using a hydrous plasma could solve the growth and leakage deterioration due to the enhanced chemisorption between the MO precursor and the hydroxylated Pt surface. Similarly, the hydroxylation passivation method for a Ge surface was reported to reduce the fast and slow interface states before Al₂O₃ ALD deposition.[14] In this work, the effects of in situ H₂O prepulse treatment on the bottom Pt electrode prior to ALD are investigated for the MIM capacitors for the first time.

## Experimental

n-Type Si wafers with a resistivity of 1–10 Ω cm with an ∼150 nm thick thermal SiO₂ layer were used as substrates. Due to poor adhesion ability between Pt and SiO₂, an ∼6 nm Ti thin film was used as an adhesion layer by electron-beam evaporation. Then, the wafers were immediately placed into the ALD chamber, a hot-wall reactor, at 250°C, and baked for 5 min to desorb all O and C residuals. Prior to the HfO₂ deposition, the H₂O prepulse treatments were employed with different cycles of 5, 20, 40, 80, and 120 as well as the control sample without the H₂O prepulse treatment. The duration time and pulse pressure of each H₂O pulse were 0.06 s and 0.1 Torr, respectively. High purity Ar was used as a purge gas with a time of 10 s between each H₂O prepulse cycle.[14] After that, HfO₂ ALD for 200 cycles was carried out with alternating pulses of Hf[N(CH₃)(C₂H₅)]₄ (TEMAH) heated at 110°C and H₂O precursors with Ar carrier gas. The process temperature and pressure were 250°C and 0.2 Torr, respectively. Finally, a layer of Pt was deposited and patterned as top electrodes by a shadow mask with a circle area of $5 \times 10^{-3}$ cm². The isopropyl alcohol/hydrofluoric acid (IPA/ HF) as etchants to etch HfO₂ was used to define the bottom electrode.

The MIM capacitors were examined by cross-sectional transmission electron microscopy (TEM) with an operating voltage of 200 kV. The chemical composition and the bonding configuration were determined by Pt4f spectra in the X-ray photoelectron spectroscopy (XPS). The X-ray source is Al Kα radiation ($h\nu$ = 1486.6 eV). The binding energies were calibrated by the C1s peaks at 284.6 eV. Atomic force microscopy (AFM) was used to identify the surface roughness of the HfO₂ films. Capacitance–voltage ($C$–$V$) measurements were performed at frequencies from 1 kHz to 1 MHz. Grazing incidence X-ray diffraction (GIXRD) was used to analyze the crystalline structure of the HfO₂ films. Cu Kα line at λ = 0.154 nm was used as the source for diffraction. Current density–voltage ($J_g$–$V$) was measured at room temperature.

## Results and Discussion

Figure 1a shows a schematic structure of our Pt/HfO₂/Pt MIM capacitor. The TEM images in Figs. 1b and 1c show the different crystalline nature and film thickness of the HfO₂ layers with the no-prepulsed sample and the 5-cycle prepulsed sample, respectively.

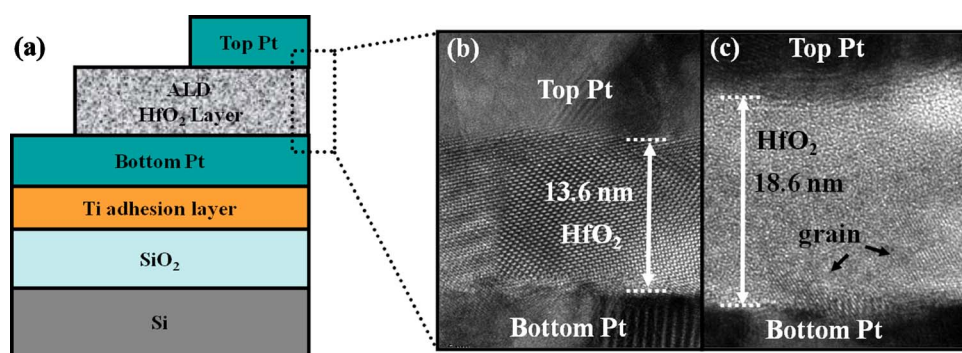* Electrochemical Society Active Member.
z E-mail: chee@cc.ee.ntu.edu.tw

**Figure 1.** (Color online) (a) Schematic structure of a Pt/HfO$_2$/Pt MIM capacitor. TEM images of (b) a no-prepulsed sample and (c) a 5-cycle prepulsed sample. The images show a distinct crystalline nature in HfO$_2$ layers.

In Fig. 1b, the HfO$_2$ layer was mainly polycrystallized. When 5 cycles of the H$_2$O prepulse treatment were applied prior to the HfO$_2$ ALD process, the polycrystallization was effectively suppressed, though a small fraction of polycrystalline grains were still found (see Fig. 1c). Figure 2 shows the GIXRD spectra of the no-prepulsed and 5-cycle prepulsed samples. Beside the face-centered cubic structure of the bottom Pt electrode, the monoclinic phase was observed to exist predominantly in the HfO$_2$ layer grown on the no-prepulsed Pt surface. With 5-cycle H$_2$O treatment on Pt, the HfO$_2$ layer is mainly amorphous (confirmed by TEM). The rich crystallinity observed in the no-prepulsed sample indicates that a chemical vapor deposition-like growth mechanism may occur due to the nucleation in the initial stage.[13]

The thickness of the 5-cycle prepulsed sample is around 18.6 nm, very similar to that of the 120-cycle prepulsed sample (18.7 nm, not shown here). It gives a deposition rate of 0.093 nm/cycle, which is consistent with the ideal value for HfO$_2$ by the ALD technique.[15] However, in the case of no-prepulsed sample, the TEM thickness and the deposition rate are reduced to be 13.6 nm and 0.068 nm/cycle, respectively. The preference of the MO precursor to bond with –OH as compared to the bare Pt surface is responsible for this. Additionally, for both cases, there are no interfacial layers between the HfO$_2$ layer and the bottom Pt electrode.

In order to investigate the effects of the H$_2$O prepulse on the surface composition of the Pt films, thinner HfO$_2$ layers with 80 ALD cycles were used for the XPS measurement. Figure 3a shows the Pt4f XPS spectra with different cycles of H$_2$O prepulse treatment. After deconvolution, it is found that the Pt4f$_{7/2}$ peaks are composed of two peaks at 71.4 and 72.3 eV, assigned to [Pt] and [PtO] bonding states, respectively. These results are consistent with the previous report.[16] The integrated intensity ratio of [PtO] to [Pt] ($I_{[PtO]}/I_{[Pt]}$) with different cycles of H$_2$O prepulse treatment is shown in Fig. 3b. The ratio of $I_{[PtO]}/I_{[Pt]}$ drastically increases to 61% for the 80-cycle prepulsed sample, which reveals that the surface of the bottom Pt electrode is effectively hydroxylated. However, the ratio of $I_{[PtO]}/I_{[Pt]}$ seems to be 70% saturated, even though the prepulse cycles increase to 120. Combining the XPS data with the aforementioned TEM results, the hydroxylated surface of the Pt electrode even with 5 cycles of the H$_2$O prepulse treatment seems to favor the amorphous growth of the subsequent HfO$_2$ deposition.

The root-mean-square roughness measured by AFM decreases from 1.05 to 0.60 nm as the prepulse treatment increases from zero cycle to 80 cycles (Fig. 4). With further increase of prepulse cycles to 120, no further improvement on the surface roughness is observed.

The C–V characteristics of the Pt/HfO$_2$/Pt MIM capacitors were measured at 100 kHz and at room temperature (Fig. 5). Correlated with the physical thickness from TEM images, the dielectric constant κ of the HfO$_2$ dielectric is estimated to be ∼19 for all the samples. The H$_2$O prepulse treatment does not affect the dielectric constant, and the decrease of capacitance densities observed in Fig. 5 is only due to the different dielectric thicknesses between the no-prepulsed and H$_2$O-prepulsed samples.

Generally, the relationship between capacitance and voltage of the MIM capacitors can be expressed as a second order polynomial equation[17]
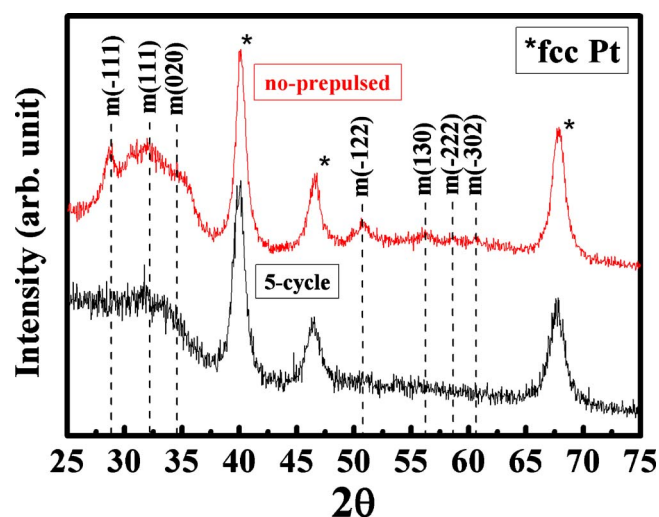


**Figure 2.** (Color online) GIXRD spectra of the HfO$_2$ films with no-prepulsed and 5-cycle prepulsed samples.
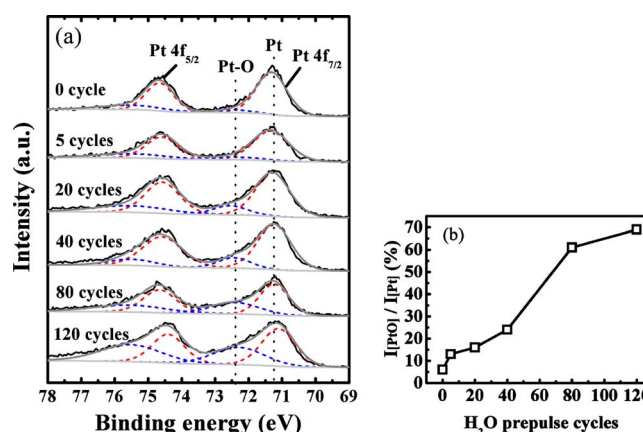


**Figure 3.** (Color online) (a) Deconvoluted Pt4f XPS spectra with different H$_2$O prepulse cycles. (b) The percentage of integrated intensity ratio of [PtO] to [Pt] as a function of the number of H$_2$O prepulse cycles.
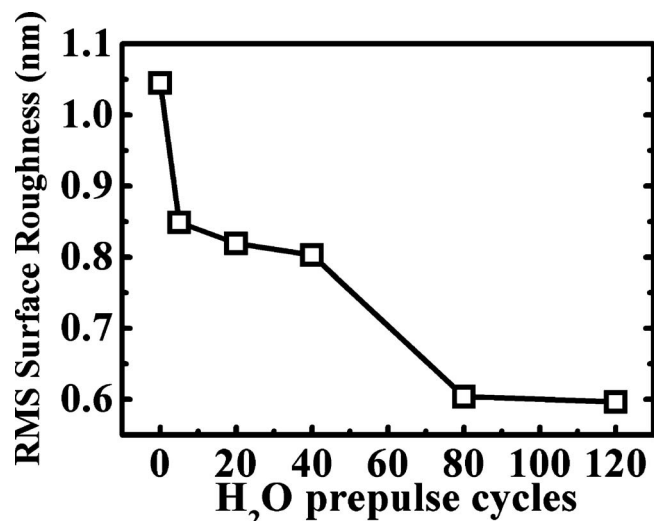
**Figure 4.** Surface roughness of the HfO$_2$ films with different H$_2$O prepulse cycles.



**Figure 6.** The extracted quadratic VCC α of the HfO$_2$ MIM capacitors as a function of H$_2$O prepulse cycles on the bottom Pt electrode.

$$\frac{\Delta C}{C_0} \times 10^6 = \left[\frac{C(V) - C_0}{C_0}\right]_{ppm} = \alpha V^2 + \beta V \qquad [1]$$

where $C_0$ is the capacitance at zero bias and α and β are the quadratic voltage coefficient of capacitance (VCC) and linear voltage coefficient of capacitance, respectively. The linear VCC β can be minimized by an adequate circuit design.[18] However, the quadratic VCC α shows a deep voltage dependence. The inset in Fig. 5 shows the normalized capacitance as a function of the positive applied voltage. As the H$_2$O prepulse cycles increase, the capacitance densities are less voltage-dependent. Figure 6 shows the extracted VCC α as a function of the prepulse cycles. The α value reduces gradually from 1810 ppm/V$^2$ for the no-prepulsed sample to 499 ppm/V$^2$ for the 120-cycle prepulsed sample. It has been reported that the voltage nonlinearity in the MIM capacitors can be caused by an electrode polarization mechanism.[19] In this proposed model, oxygen vacancies play an important role to form the accumulation layer near the electrodes, which is caused by the migration of the oxygen vacancies. Such an accumulation layer can lead to a voltage-dependent
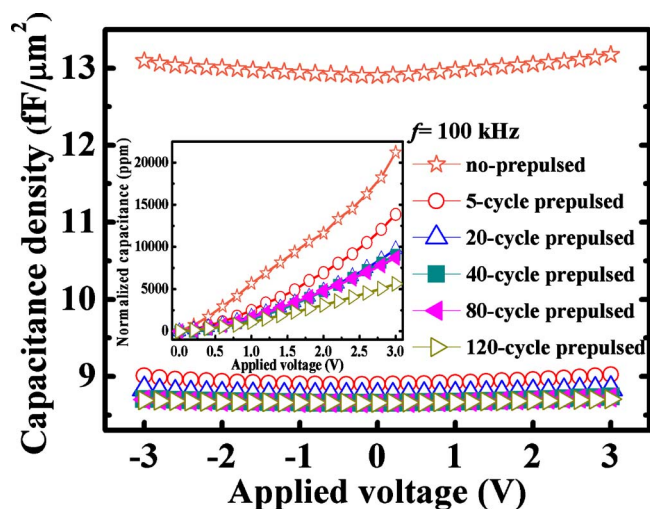
double-layer capacitance.[20] It is well known that oxygen vacancies can be inherently created during the growth in high-κ materials. Thus, it is suggested that less oxygen vacancies exist in the HfO$_2$ film when it is deposited on Pt with the H$_2$O prepulse treatment. Additionally, the α values can be improved after the annealing process, while the capacitance densities slightly decrease in an O$_2$ ambient from 400 to 800°C.

Figure 7 shows the capacitance density measured at zero bias ($C_0$) as a function of frequency for different samples. It can be seen that the capacitance density of the no-prepulsed sample exhibits a prominent frequency dispersion, indicating that the oxygen vacancies are probably created in the HfO$_2$ film. Conversely, the HfO$_2$ MIM capacitors with the H$_2$O prepulse treatment have a nearly dispersion-free response. More prepulse cycles give less dispersive $C$–$V$ characteristics.

The extracted quadratic VCC α as a function of measured frequency is shown in Fig. 8, which depicts that the α values reduce when the cycle number of the prepulse treatment increases. Smaller α are observed at higher frequency, probably due to the slow time constant of traps in the HfO$_2$ films.[7]

Figure 9 is the leakage current density $J_g$ versus the applied voltage with various prepulse cycles measured at room temperature. $J_g$ reduces from $1.3 \times 10^{-6}$ to $4.8 \times 10^{-8}$ A/cm$^2$ at 1 V for the no-



**Figure 5.** (Color online) $C$–$V$ characteristics of the HfO$_2$ MIM capacitors with different H$_2$O prepulse cycles on the bottom Pt electrode measured at room temperature and at 100 kHz. The inset shows the corresponding normalized capacitance as a function of positive applied voltage.
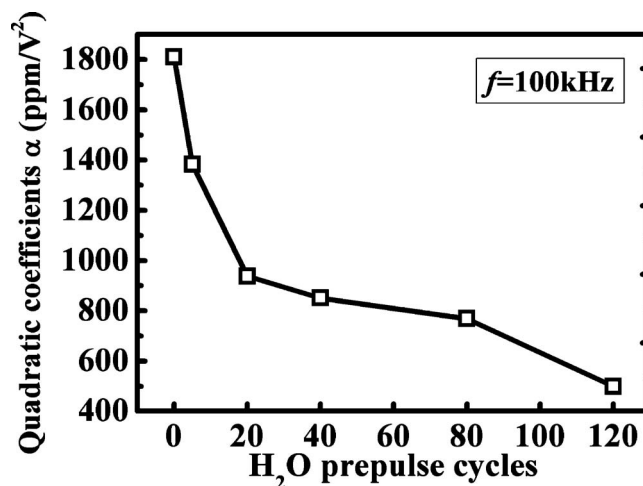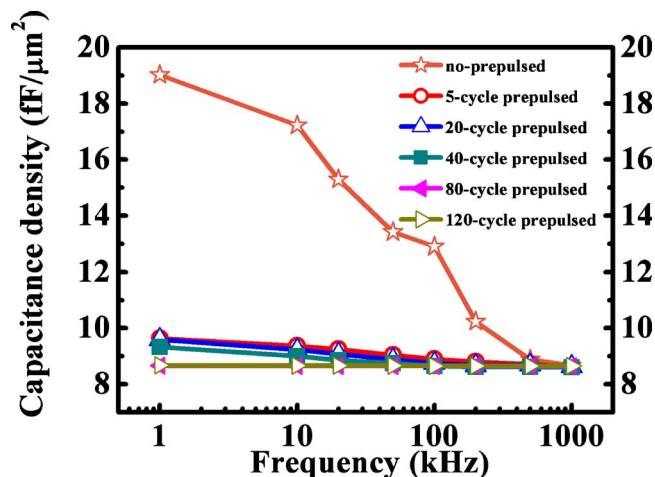


**Figure 7.** (Color online) Frequency dependence of the capacitance densities of the HfO$_2$ MIM capacitors measured at room temperature.

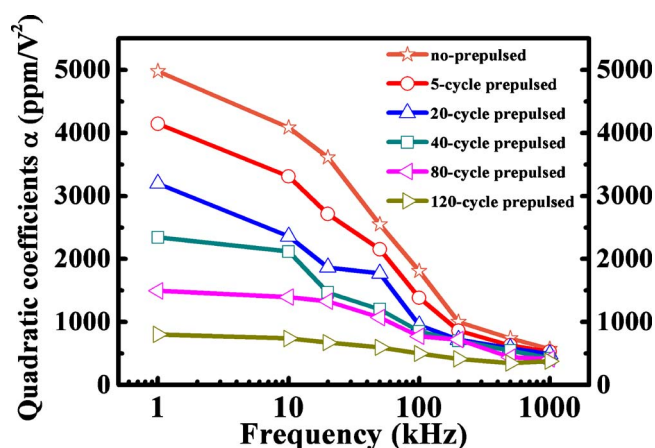**Figure 8.** (Color online) Frequency dependence of the extracted quadratic VCC α of the HfO$_2$ MIM capacitors measured at room temperature.

prepulsed to the 120-cycle prepulsed samples. There is almost 2 order of magnitude reduction. The suppression of polycrystallization observed in TEM images may be responsible for the leakage reduction through grain boundaries. Cheng et al.[21] reported that a lower leakage can be realized by a smoother interface observed in AFM results. The decrease in the surface roughness between the top Pt electrode and the HfO$_2$ layer may also account for the slight reduction of $J_g$ with the increasing prepulse cycles.

The asymmetry in the $J_g$–$V$ curve was reported previously due to the difference in the interface roughness.[22] In our study, the symmetric $J_g$–$V$ characteristics are observed in all the samples, indicating that both the top electrode and the bottom electrode have the same interface quality.
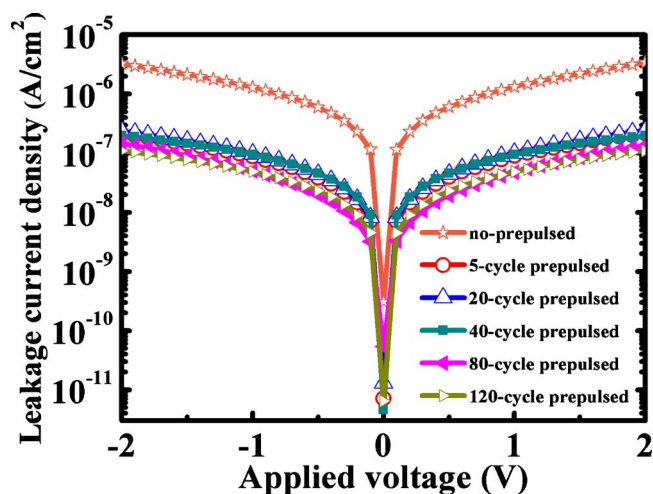


**Figure 9.** (Color online) Room temperature $J_g$–$V$ characteristics of the HfO$_2$ MIM capacitors with different cycles of H$_2$O prepulse treatment on the bottom Pt electrode.

## Conclusions

The effects of in situ H$_2$O prepulse treatment on the bottom electrode prior to the ALD process in an MIM capacitor were investigated for the first time. The material analysis showed that the hydroxylated surface of the bottom Pt electrode is favorable for growing amorphous HfO$_2$ films with less oxygen vacancies. The 5-cycle H$_2$O prepulse yielded a thicker HfO$_2$ layer ($\sim$18.6 nm) than the no-prepulsed sample ($\sim$13.6 nm). The extracted quadratic VCC α and the leakage current density can be significantly reduced to be 499 ppm/V$^2$ and $4.8 \times 10^{-8}$ A/cm$^2$, respectively. Our work proposed an effective method to improve the electrical performance of the high-κ MIM capacitors for DRAM, analog, and rf devices applications.

## References

1. International Technology Roadmap for Semiconductors (2007).
2. P. Zurcher, P. Alluri, P. Chu, P. Duvallet, C. Happ, R. Henderson, J. Mendonca, M. Kim, M. Petras, M. Raymond, et al., *Tech. Dig. - Int. Electron Devices Meet.*, **2000**, 153.
3. M. Armacost, A. Augustin, P. Felsner, Y. Feng, G. Friese, J. Heidenreich, G. Hueckel, O. Prigge, and K. Stein, *Tech. Dig. - Int. Electron Devices Meet.*, **2000**, 157.
4. J. A. Babcock, S. G. Balster, A. Pinto, C. Dirnecker, P. Steinmann, R. Jumpertz, and B. El-Kareh, *IEEE Electron Device Lett.*, **22**, 230 (2001).
5. G. D. Wilk, R. M. Wallace, and J. M. Anthony, *J. Appl. Phys.*, **89**, 5243 (2001).
6. H. Hu, C. Zhu, Y. F. Lu, M. F. Li, B. J. Cho, and W. K. Choi, *IEEE Electron Device Lett.*, **23**, 514 (2002).
7. X. Yu, C. Zhu, H. Hu, A. Chin, M. F. Li, B. J. Cho, D. L. Kwong, P. D. Foo, and M. B. Yu, *IEEE Electron Device Lett.*, **24**, 63 (2003).
8. S. J. Kim, B. J. Cho, M. F. Li, X. Yu, C. Zhu, A. Chin, and D. L. Kwong, *IEEE Electron Device Lett.*, **24**, 387 (2003).
9. Ch. Wenger, M. Lukosius, H.-J. Müssig, G. Ruhl, S. Pasko, and Ch. Lohe, *J. Vac. Sci. Technol. B*, **27**, 286 (2009).
10. C. Jorel, C. Vallée, E. Gourvest, B. Pelissier, M. Kahn, M. Bonvalot, and P. Gonon, *J. Vac. Sci. Technol. B*, **27**, 378 (2009).
11. J. J. Yang, J. D. Chen, R. Wise, P. Steinmann, Y. C. Yeo, and C. Zhu, *IEEE Electron Device Lett.*, **30**, 1033 (2009).
12. C. K. Huang and T. B. Wu, *Appl. Phys. Lett.*, **83**, 3147 (2003).
13. C. H. Chang, Y. K. Chiou, C. W. Hsu, and T. B. Wu, *Electrochem. Solid-State Lett.*, **10**, G5 (2007).
14. S. Swaminathan, Y. Oshima, M. A. Kelly, and P. C. McIntyre, *Appl. Phys. Lett.*, **95**, 032907 (2009).
15. D. M. Hausmann, E. Kim, J. Becker, and R. G. Gordon, *Chem. Mater.*, **14**, 4350 (2002).
16. G. M. Bancroft, I. Adams, L. L. Coatsworth, C. D. Bennewitz, J. D. Brown, and W. D. Westwood, *Anal. Chem.*, **47**, 586 (1975).
17. K. C. Chiang, C. C. Huang, H. C. Pan, C. N. Hsiao, J. W. Lin, I. J. Hsieh, C. H. Cheng, C. P. Chou, A. Chin, H. L. Hwang, et al., *J. Electrochem. Soc.*, **154**, G54 (2007).
18. K. S. Tan, S. Kiriake, M. DeWit, J. W. Fattaruso, C. Y. Tsay, W. E. Matthews, and R. K. Hester, *IEEE J. Solid-State Circuits*, **25**, 1318 (1990).
19. P. Gonon and C. Vallée, *Appl. Phys. Lett.*, **90**, 142906 (2007).
20. F. El Kamel, P. Gonon, and C. Vallée, *Appl. Phys. Lett.*, **91**, 172909 (2007).
21. C. H. Cheng, H. H. Hsu, I. J. Hsieh, C. K. Deng, Albert Chin, and F. S. Yeh, *Electrochem. Solid-State Lett.*, **13**, H112 (2010).
22. S. Blonkowski, M. Regache, and A. Halimaoui, *J. Appl. Phys.*, **90**, 1501 (2001).